Studies of Gold Nanoparticles as Precursors to Printed Conductive Features for Thin-Film Transistors

Yiliang Wu, Yuning Li, Ping Liu, Sandra Gardner, and Beng S. Ong*

Material Design and Integration Laboratory, Xerox Research Centre of Canada, Mississauga, Ontario L5K 2L1, Canada

Received May 17, 2006. Revised Manuscript Received July 20, 2006

Gold nanoparticles stabilized with various alkanethiols were studied as printable precursors for fabricating electrically conductive elements for printed electronics. Gold nanoparticle features were printed using stencil and microcontact techniques and then converted to highly conductive features for thin-film transistors (TFTs) at relatively low annealing temperatures. TFT devices with printed source/drain electrodes of this nature exhibited similar or better field-effect transistor (FET) characteristics than those with vacuum-evaporated gold electrodes. The improved performance was attributable to the presence of alkanethiol stabilizers on the printed electrode surface, which enabled intimate electrode/semiconductor interfacial interactions. Different alkanethiol stabilizers exerted different effects on the decomposition profiles of gold nanoparticles but not on FET performance.

Introduction

Printed thin-film transistors (TFTs) are potentially low-cost alternatives to silicon-based technology for use in large-area, ultra-low-cost, and flexible electronics where high processing speeds are not required. Most of the research activities in this area have been devoted to developing solution-processable semiconductor materials,[1−5] while prior to our work, there were only scattered studies on equally important printable conductive materials for TFTs. The source/drain electrodes, among other conductive elements, are as critical as the semiconductor for the proper functioning of TFTs. First, they have to be solution processable to enable printable TFTs, and their deposition needs to be chemically and physically inert to the semiconductor and gate dielectric to preserve the structural and electrical integrity of TFTs. Second, they have to form ohmic contact with the semiconductor to enable efficient charge carrier injection. Last but not least, they have to be operationally stable to sustain long operation life.

Earlier works on printable conductors have largely focused on conductive polymers (e.g., PEDOT/PSS,[6,7] polyanilines,[8] and polypyroles[9]) and conductive composites (e.g., polyanilines doped with carbon nanotubes[10] and conductive carbon pastes[11]). These are generally low-conductivity materials (<3 S cm^{-1}), which may also be beset with chemical, thermal, and electrical instability complications. On the other hand, noble metals such as gold and silver, which possess high electrical conductivity ($\sim 10^5$ S cm^{-1}) and operational stability, require high temperature/high vacuum deposition techniques, thereby overshadowing the low-cost benefit of printed TFTs. Electroless plating of silver has been used with micro-contact patterning for fabricating TFT electrodes,[12] but this approach may be too complex to be of practical value. Conductive silver pastes generally exhibit low thin-film conductivity, even at high annealing temperatures (>200 °C),[13] while inkjet printed silver nanoparticle features only gave high conductivity at very high annealing temperatures (>300 °C).[14] Only most recently have conductive features printed from silver nanoparticles been shown to be potentially useful for low-cost TFT application.[15,16]

Gold nanoparticles were independently investigated by us[17] and another group[18] as solution-processed high-conductivity electrical conductors. In our preliminary study, alkanethiol-stabilized gold nanoparticles were utilized as printable precursors to highly conductive elements at low annealing temperatures.[17] Gold is a particularly appealing electrode

* Corresponding author. E-mail: Beng.Ong@xrcc.xeroxlabs.com.

(1) Ong, B. S.; Wu, Y.; Liu, P.; Gardner, S. *J. Am. Chem. Soc.* **2004**, *126*, 3378.
(2) Ong, B. S.; Wu, Y.; Liu, P.; Gardner, S. *Adv. Mater.* **2005**, *17*, 1141.
(3) Wu, Y.; Li, Y.; Gardner, S.; Ong, B. S. *J. Am. Chem. Soc.* **2005**, *127*, 614.
(4) Meng, H.; Zheng, J.; Lovinger, A. J.; Wang, B.-C.; Gregory Van Patten, P.; Bao, Z. *Chem. Mater.* **2003**, *15*, 1778.
(5) Wu, Y.; Liu, P. Gardner, S.; Ong, B. S. *Chem. Mater.* **2005**, *17*, 221.
(6) Sirringhaus, H.; Kawasem, T.; Friend, R. H.; Shimoda, T.; Inbasekaran, M.; Wu, W.; Woo, E. P. *Science* **2000**, *290*, 2123.
(7) Halik, M.; Klauk, H.; Zschieschang, U.; Schmid, G.; Radlik, W.; Werner, W. *Adv. Mater.* **2002**, *14*, 1717.
(8) Drury, C. J.; Mutsaers, C. M. J.; Hart, C. M.; Maters, M.; de Leeuw, D. M. *Appl. Phys. Lett.* **1998**, *73*, 108.
(9) Koezuka, H.; Tsumura, A.; Fuchigami, H.; Kuramoto, K. *Appl. Phys. Lett.* **1993**, *62*, 1794.
(10) Lefenfeld, M.; Blanchet, G.; Rogers, J. A. *Adv. Mater.* **2003**, *15*, 1188.
(11) Brandon, E. J.; West, W. Wesseling, E. *Appl. Phys. Lett.* **2003**, *83*, 3945.
(12) Tate, J.; Rogers, J. A.; Jones, C. D. W.; Vyas, B.; Murphy, D. W.; Li, W.; Bao, Z.; Slusher, R. E.; Dodabalapur, A.; Katz, H. E. *Langmuir* **2000**, *16*, 6054.
(13) Gray, C.; Wang, J.; Duthaler, G.; Ritenour, A.; Drzaic, P. *Proc. SPIE* **2001**, *No. 4466*, 89.
(14) Fuller, S. B.; Wilhelm, E. J.; Jacobson, J. M. *J. Microelectromech. Syst.* **2002**, *11*, 54.
(15) Li, Y.; Wu, Y.; Ong, B. S. *J. Am. Chem. Soc.* **2005**, *127*, 3266.
(16) Wu, Y.; Li, Y.; Ong, B. S. *J. Am. Chem. Soc.* **2006**, *128*, 4202.
(17) Wu, Y.; Li, Y.; Ong, B. S.; Liu, P.; Gardner, S.; Chiang, B. *Adv. Mater.* **2005**, *17*, 184.
(18) Huang, D.; Liao, F.; Molsesa, S.; Redinger, D.; Subramanian, V. *J. Electrochem. Soc.* **2003**, *150*, G412.

10.1021/cm0611643 CCC: $33.50
Published on Web 08/26/2006

material for organic p-channel TFTs as it forms excellent ohmic contact with most p-type organic semiconductors (e.g., regioregular polythiophenes) and is operationally stable. In this paper, we present our detailed studies on gold nanoparticles with different stabilizers, their morphological behaviors under thermal stimulation as observed by SEM and AFM techniques, and their electrical properties and performance as printed source/drain electrodes in TFTs.

Experimental Section

Materials. Poly(3,3‴-didodecylquaterthiophene), PQT-12,[1] was used as the semiconductor for the TFT test devices. Alkanethiol-stabilized gold nanoparticles were prepared via a modified procedure of a literature method[19] as follows.

Au-C_4 (1-butanethiol-stabilized gold nanoparticles): To a solution of tetraoctylammonium bromide (8.75 g, 16 mmol) in 300 mL of toluene in a 2-L flask was added a solution of $HAuCl_4 \cdot 3H_2O$ (1.57 g, 4 mmol) in 150 mL of water with rapid stirring. After 2 min, 1-butanethiol (0.36 g, 4 mmol) in 50 mL of toluene was added with vigorous stirring for 10 min at room temperature before the mixture was cooled down to 0 °C with an ice-water bath. A freshly prepared solution of $NaBH_4$ (1.51 g, 40 mmol) in 100 mL of water was then added to the vigorously stirred reaction mixture at 0 °C over a period of 30 s, and the resultant mixture was vigorously stirred for 3 h. The organic phase was separated, washed with water three times, dried with anhydrous $MgSO_4$, and filtered. The filtrate was concentrated to 50 mL by evaporation at reduced pressure (<50 °C) and added dropwise to 200 mL of vigorously stirred methanol. The precipitated solid was collected by centrifugation, vacuum-dried, and then dissolved in 20 mL of cyclohexane. The resultant solution was added dropwise to 200 mL of vigorously stirred methanol and left to settle over a period of 1 h, and the black solid product was collected by centrifugation and dried in vacuo. Yield: 0.81 g.

Au-C_8 (1-octanethiol-stabilized gold nanoparticles): Au-C_8 was prepared in a similar manner by using 0.78 g (2 mmol) of $HAuCl_4 \cdot 3H_2O$, 4.37 g (4 mmol) of tetraoctylammonium bromide, 0.59 g (4 mmol) of 1-octanethiol, and 0.76 g (20 mmol) of $NaBH_4$. Yield: 0.39 g.

Au-C_{12} (1-dodecanethiol-stabilized gold nanoparticles): Au-C_{12} was prepared in a similar manner by using 0.78 g (2 mmol) of $HAuCl_4 \cdot 3H_2O$, 4.37 g (4 mmol) of tetraoctylammonium bromide, 0.81 g (4 mmol) of 1-dodecanethiol, and 0.76 g (20 mmol) of $NaBH_4$. Yield: 0.48 g.

Instruments. Thin-film absorption spectra were obtained on a VARIAN CARY 5 UV−vis−NIR spectrophotometer. Thermogravimetric analysis was conducted on a TA Instrument SDT 2960 simultaneous DTA-TGA with a rate of 5 °C/min. X-ray diffraction was performed on a Rigaku MiniFlex diffractometer using Cu Kα radiation (λ 1.5418 Å) with a $\theta-2\theta$ scans configuration. SEM was measured on a JEOL 6300F FE-SEM with an accelerating voltage of 10 kV. Transmission electron microscopy (TEM) was obtained on a JEOL 2010F (S)TEM with an accelerating voltage of 200 kV using a gold nanoparticle sample deposited on a carbon-coated copper grid. AFM was taken on PH-47 (NT-MDT) at room temperature in semi-contact mode. Thin-film conductivity was measured on a Keithley 237 high voltage source measure unit using a conventional four-probe technique.

TFT Fabrication and Characterization. A bottom-gate, bottom-contact TFT configuration was used as our test device structure with the source/drain electrodes fabricated from gold nanoparticles. A heavily *n*-doped silicon wafer was used as a substrate and gate electrode, while its SiO_2 surface layer (∼110 nm) served as the gate dielectric (capacitance ∼32 nF/cm^2). The silicon wafer was first cleaned with isopropanol, argon plasma, isopropanol, and air-dried, and then modified with octyltrichlorosilane (OTS-8) by immersing in a 0.1 M solution of octyltrichlorosilane (OTS-8) in toluene at 60 °C for 20 min. Subsequently, the wafer was washed with toluene and isopropanol and air-dried. The gold nanoparticles were deposited on the modified SiO_2 surface by stencil printing or microcontact printing to form gold nanoparticle source/drain electrode features as described herein. For stencil printing, a concentrated solution of gold nanoparticles in a high boiling solvent such as dichlorobenzene was most desirable. A 13-μm stainless stencil patterned with an array of source/drain electrode feature gaps was first laid on top of a substrate such as silicon wafer. A strong magnet was positioned on the other side of the substrate to hold the stencil tightly onto the substrate to minimize the gap between the stencil and the substrate to prevent ink smearing and leakage, A dispersion or solution of 20 wt % of gold nanoparticles in 1,2-dichlorobenzene was used as the printing ink composition. The gold nanoparticle ink was painted through the electrode feature gaps of the stencil onto the substrate with a fine paint brush. After drying at room temperature for 15−30 min, the stencil was removed, thus leaving an array of printed gold nanoparticle electrode features on the substrate. For microcontact printing, a PDMS stamp carrying embossed source/drain electrode features was utilized. The surface of PDMS stamp was first cleaned with oxygen plasma and then modified with a self-assembled monolayer of OTS-8 to create a low surface-energy electrode surface to enable efficient release of gold nanoparticle ink during printing. A 5−10 wt % gold nanoparticles solution in cyclohexane was spin coated on the PDMS stamp surface. The PDMS stamp carrying the gold-coated nanoparticle ink was lightly pressed against the substrate surface for 30 s and then lifted, thus leaving an array of printed of gold nanoparticle electrode features on the substrate. Subsequent annealing on a hotplate for about 5−30 min resulted in the formation of a series of electrically conductive source/drain electrode pairs. Finally, a 30 nm thick sample of the PQT-12 semiconductor layer was deposited by spin coating a 0.3 wt % of PQT-12 nanoparticle dispersion in dichlorobenzene[2] and annealed at 140 °C for ∼15 min. For comparison, both a top- and a bottom-contact TFTs with vacuum-evaporated gold source/drain electrodes were also fabricated. These experimental TFT devices were characterized using Keithley SCS-4200 characterization system under ambient conditions. The mobilities in the saturated regime were extracted from the following equations:

$$I_D = C_i \mu (W/2L) (V_G - V_T)^2 \quad (1)$$

where I_D is the drain current, C_i is the capacitance per unit area of the gate dielectric layer, and V_G and V_T are respectively the gate voltage and threshold voltage. The V_T of the device was determined from the relationship between the square root of I_D at the saturated regime and V_G of the device by extrapolating the measured data to $I_D = 0$.

Results and Discussion

Previously, we showed that printed, electrically insulating gold nanoparticle thin films could be converted to electrically conductive gold thin films by annealing at relatively low temperatures of 140−200 °C.[17] The transformation of gold nanoparticle thin films into conductive gold thin films was

(19) Brust, M.; Fink, J.; Bethell, D.; Schiffrin, D. J.; Kiely, C. *J. Chem. Soc. Chem. Commun.* **1994**, 801.

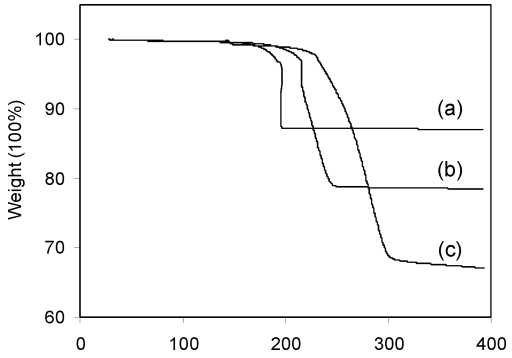

Figure 1. Thermogravimetric profiles of alkanethiol-stabilized gold nanoparticles: (a) Au-C_4; (b) Au-C_8; (c) Au-C_{12}.

investigated by absorption spectroscopy, X-ray study, and conductivity measurement. We present herein a detailed study of thermal transition behaviors of gold nanoparticles with different alkanethiol stabilizers having representative alkyl chain lengths [1-butanethiol (Au-C_4), 1-octanethiol (Au-C_8), and 1-dodecanethiol (Au-C_{12})] from electrically insulating or semiconducting to highly conductive states.

Figure 1 depicts the thermogravimetric analysis (TGA) of gold nanoparticles of similar particle sizes (~2 − 4 nm) with three different stabilizers, all showing a single-step weight-loss behavior but with different thermal profiles and onset-decomposition temperature. Au-C_4, with a 1-butanethiol stabilizer, which has the shortest alkyl chain in this series, registered the lowest onset-decomposition temperature of 140 °C and a weight-loss end point temperature of 190 °C. Increasing the stabilizer chain length led to a higher decomposition and weight-loss temperatures, which are in line with the expectation based on the boiling points of alkanethiol stabilizers [1-butanthiol (98 °C); 1-octanethiol (197−200 °C); 1-dodecanethiol (266 − 286 °C)]. However, the shapes of their decomposition profiles were different. While Au-C_4 displayed a sharp weight-loss profile, both Au-C_8 and Au-C_{12} displayed a somewhat gradual decomposition and weight loss over a wide temperature range. This could be attributed largely to the phenomenon of size evolution of gold nanoparticles, which was observed to be particularly pronounced with longer alkanethiol stabilizer.[20] In the case of Au-C_4, the 1-butanethiol stabilizer was mostly evaporated due to its low boiling point during the TGA heating scan before the complete collapse of gold nanoparticles into a continuous phase, thus a sharp decomposition/weight loss temperature. On the other hand, with a high boiling-point stabilizer, size evolution from small to larger particles from heat-induced coalescence of nanoparticles occurred during heating. This led to a gradual formation of a continuous phase from collapsed nanoparticles with simultaneous release of stabilizer molecules over a temperature range.

Figure 2, panels a and b, gives the TEM images of two Au-C_8 thin films, showing respectively an as-prepared multilayer film of discrete gold nanoparticles on a copper grid and the formation of nanostructural networks of coalesced gold nanoparticles after annealing at 160 °C in a vacuum oven. Since this film was only a few layers thick

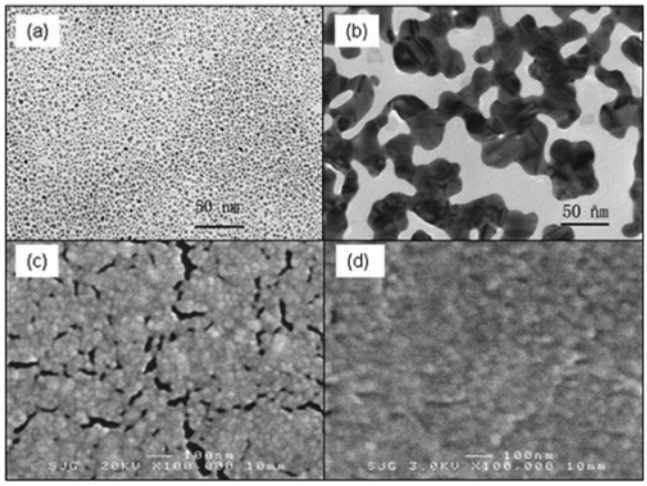

Figure 2. (a) TEM image of a multilayer film of Au-C_8 on copper grid. (b) TEM image of an annealed multilayer film of Au-C_8, showing nanonetwork structures of coalesced gold nanoparticles. (c) SEM image of a 40-nm annealed Au-C_4 film. (d) SEM image of a 60-nm annealed Au-C_4 film.

(as revealed by TEM), thus significant amounts of voids were present in the annealed thin film. A continuous thin film with full coverage could be obtained by increasing film thickness, as in the case of for example a 40 nm thick film with a few scattered voids (Figure 2c) and a 60 nm thick film with no visible voids (Figure 2d). Figure 3 shows the AFM topography images of randomly selected 10 × 10 μm areas of two Au-C_4 thin films (~80 nm) annealed under different conditions. Both of these films show uniform surface coverage with excellent continuous coalesced particle-to-particle contacts with no visible signs of cracks, thus enabling achievement of excellent electrical conductivity characteristics.

The electrical conductivity of thin films was measured by the traditional four probe technique. Table 1 summarizes the electrical conductivity of various gold nanoparticle thin films before and after annealing at 200 °C. The conductivity of as-prepared gold nanoparticle thin films was inversely correlated with the alkanethiol stabilizer chain length, which was expected since electrical conduction is through tunneling[21] and a longer alkanethiol stabilizer would be more insulative. Upon annealing, all three nanoparticle films exhibited dramatically improved conductivity approaching that of a vacuum-evaporated gold thin film. The conductivity achievable with these gold nanoparticle films was several orders of magnitude higher than those of most conductive polymer systems (e.g., PEDOT/PSS[6,7]; polyaniline/carbon nanotubes[10]). The alkanethiol stabilizer chain length exhibited a slight effect on conductivity, which decreased by a factor of 2 in magnitude when the chain length increased from 4 to 12 carbon atoms. However, a longer alkanethiol stabilizer would require a longer annealing time to achieve the saturated conductivity. Specifically, for an 80-nm gold nanoparticle film of Au-C_4, Au-C_8, and Au-C_{12}, it would require approximately 1, 15, and 30 min, respectively, to achieve the saturated conductivity at 200 °C, while a higher

(20) Teranishi, T.; Hasegawa, S.; Shimizu, T.; Miyake, M. *Adv. Mater.* **2001**, *13*, 1699.

(21) Zamborini, F. P.; Leopold, M. C.; Hicks, J. F.; Kulesza, P. J.; Malik, M. A.; Murray, R. W. *J. Am. Chem. Soc.* **2002**, *124*, 8958.

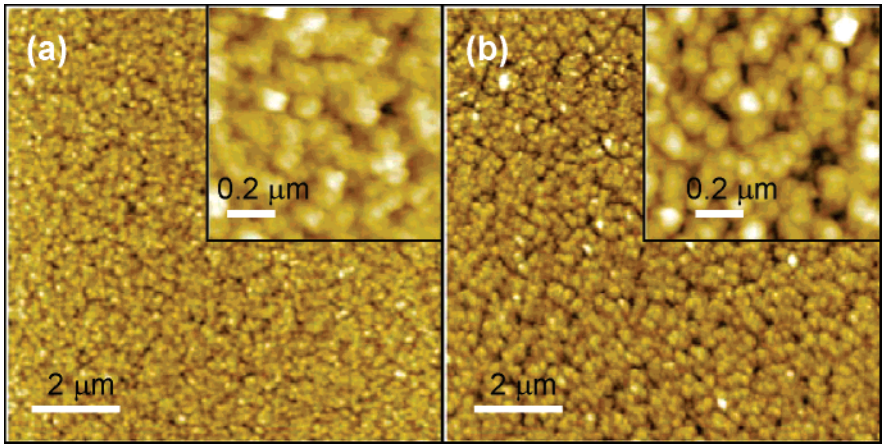

Figure 3. AFM topographic images of Au-C_4 thin films (~80 nm): (a) annealed in vacuum oven at 140 °C; (b) annealed on hotplate from room temperature to 190 °C at 30 °C min^{-1}.

Table 1. Thin Film Conductivity of Different Conductive Thin Films as Measured by Conventional Four-Probe Technique

thin film (thickness, nm)	conductivity (S cm^{-1}) before annealing	conductivity (S cm^{-1}) after annealing
Au-C_4 (60 nm)	3.2×10^{-3}	$0.5-1.0 \times 10^5$
Au-C_8 (80 nm)	8.5×10^{-6}	$5.6-7.1 \times 10^4$
Au-C_{12} (80 nm)	5.0×10^{-7}	$3.6-4.4 \times 10^4$
Au evaporation (70 nm)	2.0×10^5	
PEDOT/PSS (85 nm)	0.1	

temperature (e.g., 220 °C) reduces the annealing time without increasing conductivity.

The morphological quality of annealed gold nanoparticle film improved with its thickness as less voids and better film continuity were observed in a thinker film. Accordingly, film morphology would be expected to exhibit significant impact on film conductivity. Figure 2c shows a 40-nm annealed Au-C_4 film with extensive voids affording a conductivity of 6.0×10^3 S cm^{-1}, while a thicker 60-nm film with full coverage is shown in Figure 2d giving a conductivity as high as 1.0×10^5 S cm^{-1}.

The patterning of gold nanoparticles into electrode features was accomplished by stencil and microcontact printing (see Experimental Section). The printed nanoparticle electrode features were annealed at the required temperature to give electrically conductive gold electrodes. As reported before,[17] except for a few voids and bumps, the stencil printed electrodes displayed smooth edges throughout and good thin-film uniformity with an average thickness of about 100−125 nm, thus enabling creating uniform semiconductor channels for TFTs. With the stencil printing technique as described, TFTs with channel lengths and electrode widths down to about 60 μm could be realized. However, printing finer features remained a practical challenge for this technique. Figure 4 shows an optical image of annealed gold features from microcontact printing. This printing technique was capable of achieving finer electrode features and narrower line gaps of about 10 μm, but it was necessary to exercise care in not lifting off the printed gold nanoparticles during the release process. This complication may be minimized or overcome by optimizing the surface adhesion property of substrate material.

To evaluate the electrical performance of printed gold nanoparticle conductor, we fabricated a series of bottom-gate, bottom-contact TFTs using printed gold source/drain electrodes. Figure 5 shows the output and transfer curves of a typical TFT device with the stencil printed gold source/drain electrodes fabricated from Au-C_4. The observed field-effect transistor (FET) behaviors conformed to the conventional transistor models in both the linear and saturated regimes. Good saturation characteristics with clear saturation currents were noted in the output curves. The extracted saturation mobility was up to 0.15 cm^2 V^{-1} s^{-1} with a current on/off ratio of 10^6. On average, these bottom-contact devices afforded mobility in the range of 0.07−0.18 cm^2 V^{-1} s^{-1} with the median being ~0.13 cm^2 V^{-1} s^{-1}, which are identical to the top-contact devices with vacuum-evaporated gold electrodes. No observable differences in FET characteristics were noted for TFTs with electrodes produced by

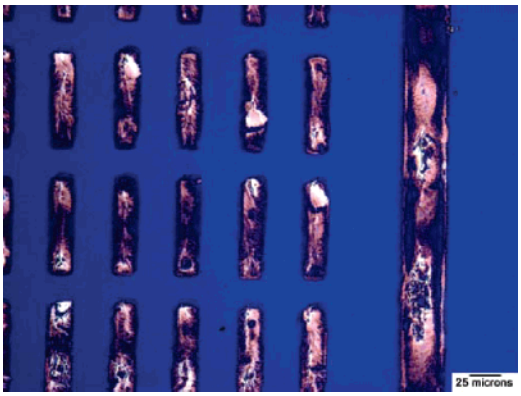

Figure 4. Optical image of microcontact printed electrodes from Au-C_8.

Table 2. FET Performance Characteristics of TFTs with Source/Drain Electrodes Printed from Different Gold Nanoparticles.

electrodes (TFT configuration)	threshold voltage (V)	mobility (cm^2 V^{-1} s^{-1})	on/off ratio
evaporated gold (top-contact)	−4	0.07−0.18	~10^6
evaporated gold (bottom-contact)	−12	0.04−0.06	~10^4
modified evaporated gold (bottom-contact)	−5	0.07−0.14	10^5-10^6
Au-C_4 (bottom-contact)	−4	0.09−0.18	10^5-10^6
Au-C_8 (bottom-contact)	−5	0.07−0.13	10^5-10^6
Au-C_{12} (bottom-contact)	−7	0.08−0.14	10^5-10^6

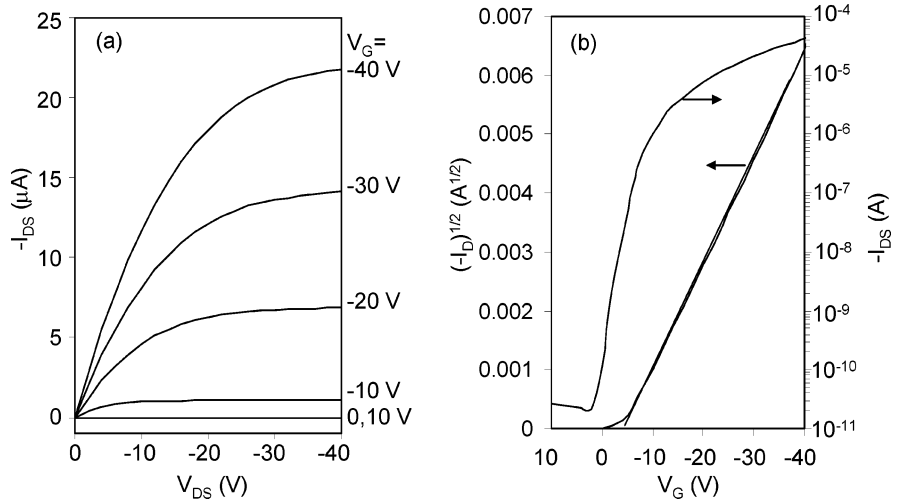

Figure 5. $I-V$ characteristics of an illustrative TFT device with printed gold source/drain electrodes using PQT-12 as channel semiconductor (channel length = 115 μm; channel width = 2700 μm). (a) Plot of drain current I_D vs source-drain voltage V_D as a function of gate voltage V_G. (b) Plot of I_D and $(-I_D)^{1/2}$ vs V_G at a constant $V_D = -60$ V (mobility and current on/off ratio extracted from this plot).

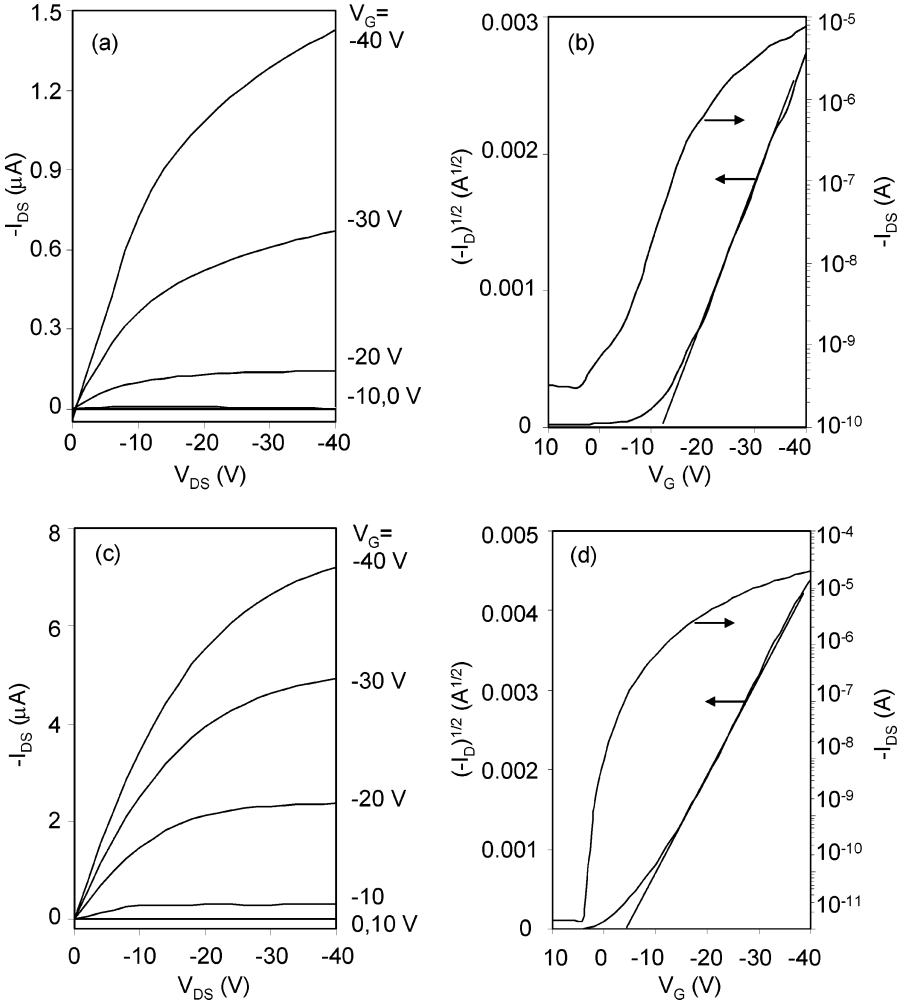

Figure 6. Bottom-contact TFTs with vacuum-evaporated gold source/drain electrodes (channel length = 90 μm; channel width = 1000 μm). Panels a and b are respective output curves and transfer characteristics of a device with non-modified gold electrodes. Panels c and d are respective output curves and transfer characteristics of a device with 1-octanethiol-modified gold electrodes.

stencil and microcontact printings. Table 2 summarizes the FET performance characteristics of TFT devices with the gold source/drain electrodes printed from different gold nanoparticles. While conductivity varied slightly, little or no difference in FET mobility and current on/off ratio were observed with different alkanethiol stabilizers. The average threshold voltage, on the other hand, showed a slight increase with increased alkanethiol stabilizer chain length. The transistors with printed gold electrodes also exhibited the same long-term stability as those employing vacuum-evaporated gold electrodes. A slight decrease in on-current and a slight increase in off-current were observed after the

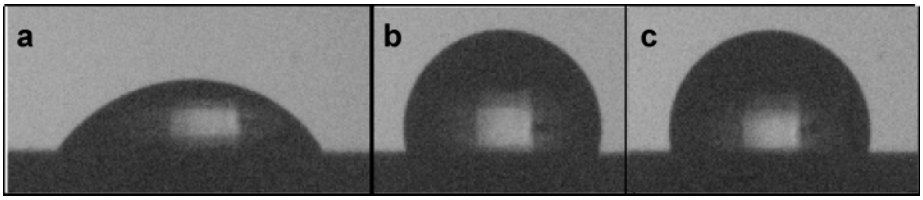

Figure 7. Water drop on various surfaces: (a) vacuum-evaporated gold thin film (contact angle ~55°), (b) vacuum-evaporated thin film modified with 1-octanethiol (contact angle ~102°), and (c) annealed Au-C_4 thin film (contact angle ~100°).

devices were stored in the dark for over 1 month. However, the same observation was also noted with the devices using vacuum-evaporated gold electrodes.

We observed that the FET properties of TFTs with printed source/drain electrodes were superior to those of bottom-contact devices with vacuum-evaporated gold electrodes (Table 2). The latter exhibited no clear saturation behaviors and larger threshold voltages (Figure 6a and b), with the extracted saturation mobility being ~0.06 $cm^2\ V^{-1}\ s^{-1}$, which is a factor of 2−3 lower than those with printed gold electrodes. The same behavior was also observed with the mobility in the linear regime. This is surprising in view of the fact that gold electrode ($\Phi = 5.1$ eV) is energetically compatible with the PQT-12 semiconductor (HOMO = 5.05 eV) and should permit establishment of excellent ohmic contact. A similar result was reported for the pentacene bottom-contact TFTs,[22] and this was attributed to the difference in morphology of pentacene semiconductor on hydrophilic gold surface and hydrophobic channel. We believe the cause of poor performance was more likely due to poor electrode/semiconductor interfacial contact since top-contact TFTs exhibited normal performance characteristics under similar conditions. Intimate interfacial contact between hydrophilic vacuum-evaporated gold electrodes (advancing water contact angle ~55°, Figure 7a) and a hydrophobic organic semiconductor is generally difficult to establish during semiconductor deposition in the bottom-contact devices. In the top-contact configuration, excellent interfacial contact can be easily achieved as the vacuum-evaporated gold electrode is continuously evaporated at atomic level onto the semiconductor, which permits interlayer penetration. The performance of bottom-contact TFTs could however be improved by modifying the gold electrodes with alkanethiol to render them hydrophobic. When an evaporated gold surface was treated with 1-octanethiol, it became hydrophobic as revealed by a higher water contact angle of 102° (Figure 7b), which would render the electrodes compatible with organic semiconductors. Figure 6, panels c and d, shows the $I-V$ characteristics of a bottom-contact TFT device with 1-octanethiol-treated vacuum-evaporated gold source/drain electrodes. This device now showed good saturation behaviors as well as much higher mobility (~0.1 $cm^2\ V^{-1}\ s^{-1}$), which was in line with those of top-contact devices with vacuum-evaporated electrodes or bottom-contact TFTs with printed gold electrodes.

The excellent performance of bottom-contact TFTs with printed gold electrodes could thus be attributed to the presence of a layer of residual alkanethiol stabilizer or its thermally transformed derivative on the surface of electrodes after annealing. The existence of residual alkanethiol or its transformed derivative on the electrode surface was conclusively affirmed by the large water contact angle (~100°) of a gold thin film generated from gold nanoparticles as shown in Figure 7c.

Conclusion

We have shown that alkanethiol-stabilized gold nanoparticles represent promising printable precursors for fabricating electrically conducting elements for printed microelectronics. Electrically conducting gold features were successfully patterned from these gold nanoparticles on appropriate substrates via stencil and microcontact printing techniques, and it is expected that they can be easily patterned by inkjet printing as well. The thin-film electrical conductivity of printed conducting elements was close to those obtained by vacuum-evaporation or to gold bulk conductivity. A post-printing conditioning step via thermal annealing at a relatively low temperature of about 140−200 °C was required to bring about the transition from printed insulting gold nanoparticle features to electrically conducting gold elements. The generally mild annealing conditions have rendered this approach highly appealing for application in printed transistor circuits, particularly on plastic substrates to enable flexible electronics. As a proof-of-concept demonstration, TFTs with printed source/drain electrodes were fabricated and shown to provide excellent FET performance characteristics.

Acknowledgment. The assistance of Ms. Ni Zhao of McMaster University in obtaining TEM images is gratefully acknowledged. Partial financial support was provided by the National Institute of Standards and Technology through an Advanced Technology Program Grant (70NANB0H3033).

CM0611643

(22) Kymissis, I.; Dimitrakopoulos, C. D.; Purushothaman, S. *IEEE Trans. Electron Devices* **2001**, *48*, 1060.